23. Badio B, Daly JW. Epibatidine, a potent analgetic and nicotinic agonist. *Mol Pharmacol* 1994;45:563–569.
24. Houghtling RA, Davila-Garcia MI, Kellar KJ. Characterization of (±)-[^{3}H]epibatidine binding to nicotinic cholinergic receptors in rat and human brain. *Mol Pharmacol* 1995;48:280–287.
25. Perry DC, Kellar KJ. ^{3}H-epibatidine labels nicotinic receptors in rat brain: an autoradiographic study. *J Pharmacol Exp Ther* 1995;275:1030–1034.
26. London ED, Scheffel U, Kimes AS, Kellar KJ. In vivo labeling of nicotinic acetylcholine receptors in brain with [^{3}H]epibatidine. *Eur J Pharm* 1995;278:R1–R2.
27. Scheffel U, Taylor GF, Kepler JA, Carroll FI, Kuhar MJ. In vivo labeling of neuronal nicotinic acetylcholine receptors with radiolabeled isomers of norchloroepibatidine. *NeuroReport* 1995;6:2483–2488.
28. Horti AG, Ravert HT, London ED, Dannals RF. Synthesis of a radiotracer for studying nicotinic acetylcholine receptors by positron emission tomography: (±)-exo-2-(2-[^{18}F]fluoro-5-pyridyl)-7-azabicyclo[2.2.1]heptane. *J Labell Comp Radiopharm* 1996; 38:355–366.
29. Riche D, Hantraye P, Guibert B, Naquet R, Loc'h C, Maziere B, Maziere M. Anatomical atlas of the baboon's brain in the orbito-meatal plane used in experimental positron emission tomography. *Brain Res Bull* 1988;20:283–301.
30. London ED, Waller SB, Wamsley JK. Autoradiographic localization of [^{3}H]nicotine binding sites in the rat brain. *Neurosci Lett* 1985;53:179–184.
31. Nordberg A, Alafuzoff I, Winblad B. Nicotinic and muscarinic subtypes in the human brain: changes with aging and dementia. *J Neurosci Res* 1992;31:103–111.
32. Horti AG, Ravert HT, Mathews WB, Musachio JL, Kimes A, London ED, Dannals RF. Synthesis of high specific activity carbon-11 N-methylated analogs of epibatidine for imaging nAChRs [Abstract]. *J Nucl Med* 1996;37:192P.
33. Cimino M, Marini P, Fornasari D, Cattabeni F, Clementi F. Distribution of nicotinic receptors in cynomologus monkey brain and ganglia: localization of alpha 3 subunit mRNA, alpha-bungarotoxin and nicotine binding sites. *Neuroscience* 1992;51:77–86.
34. Pauly JR, Marks MJ, Gross SD, Collins AC. An autoradiographic analysis of cholinergic receptors in mouse brain after chronic nicotine treatment. *J Pharmacol Exp Ther* 1991;258:1127–1136.
35. Sullivan JP, Decker MW, Brioni JD, et al. (±)-Epibatidine elicits a diversity of in vitro and in vivo effects mediated by nicotinic acetylcholine receptors. *J Pharmacol Exp Ther* 1994;271:624–631.
36. McKay J, Lindstrom J, Loring RH. Determination of nicotinic receptor subtypes in chick retina using monoclonal antibodies and 3H-epibatidine. *Med Chem Res* 1994; 4:528–537.
37. Logan J, Fowler JS, Volkow ND, et al. Graphical analysis of reversible radioligand binding from time-activity measurements applied to [N-^{11}C-methyl]-(-)-cocaine PET studies in human subjects. *J Cereb Blood Flow Metab* 1990;10:740–747.
38. Huang SC, Barrio JR, Phelps ME. Neuroreceptor assay with positron emission tomography: equilibrium versus dynamic approaches. *J Cereb Blood Flow Metab* 1987;7:214–229.
39. Wong DF, Gjedde A, Wagner HN Jr. Quantification of neuroreceptors in the living human brain. I. Irreversible binding of ligands. *J Cereb Blood Flow Metab* 1986;6: 137–146.
40. Wong DF, Gjedde A, Wagner HN Jr, Dannals RF, Douglass KH, Links JM, Kuhar MJ. Quantification of neuroreceptors in the living human brain. II. Inhibition studies of receptor density and affinity. *J Cereb Blood Flow Metab* 1986;6:147–153.
41. Gjedde A. High- and low-affinity transport of D-glucose from blood to brain. *J Neurochem* 1981;36:1463–1471.
42. Patlak CS, Blasberg RG, Fenstermacher JD. Graphical evaluation of blood-to-brain transfer constants for multiple time uptake data. *J Cereb Blood Flow Metab* 1983;3:1–7.

Technetium-99m(V)-DMSA and Thallium-201 in Brain Tumor Imaging: Correlation with Histology and Malignant Grade

Tsuneo Hirano, Hidenori Otake, Ken Kazama, Kazuki Wakabayashi, Akira Zama, Takashi Shibasaki, Masaru Tamura and Keigo Endo

Departments of Nuclear Medicine and Neurosurgery, Gunma University, School of Medicine, Maebashi, Gunma, Japan

This study was performed to compare imaging ability between pentavalent ^{99m}Tc-DMSA and ^{201}TlCl in primary and metastatic brain tumors and to evaluate the relationship between retention and histologic malignancy. **Methods:** Patients with a brain tumor were selected by MRI and/or CT. Dynamic, early and delayed static SPECT images of the brain were obtained immediately, 30 min and 3 hr after intravenous administration of approximately 555 MBq ^{99m}Tc(V)-DMSA and 111 MBq ^{201}Tl-Cl, respectively. Both studies were performed on separate days within a week. Uptake ratios, retention ratio and retention index were calculated and compared with tumor histology and malignancy grade. **Results:** One-hundred six studies were performed on 100 patients and 118 lesions were demonstrated: 16 glioblastomas, 13 anaplastic astrocytomas (Grade III), 19 astrocytomas (Grade II), 29 meningiomas, 11 schwannomas and 14 metastases. Approximately 93% and 88%, respectively, of primary and metastatic brain tumors were demonstrated by ^{99m}Tc(V)-DMSA and ^{201}TlCl. The early uptake ratios were closely related to the tumor vascularity, but had no statistically significant difference in the tumor histology or histologic malignancy on either radiopharmaceuticals. The delayed uptake ratio, retention ratio and retention index were higher in malignant tumors than benign ones on ^{99m}Tc(V)-DMSA, however, there was no statistically significant difference between benign and malignant tumors on ^{201}TlCl. **Conclusion:** Technetium-99m(V)-DMSA washout from the tumor was highly dependent upon its histology and histologic malignancy. The delayed uptake ratio, retention ratio and retention index significantly reflected tumor histology and clearly distinguished between benign and malignant tumors with a statistically significant difference. There was no statistically significant difference in ^{201}TlCl uptake or washout among the brain tumors. Technetium-99m-DMSA is superior to ^{201}TlCl in imaging quality, sensitivity to brain tumors and specificity for differentiating benign tumors from malignant ones. These results could suggest the clinical utility of ^{99m}Tc(V)-DMSA in imaging primary and metastatic brain tumors and differentiating their histological malignancy grade noninvasively.

Key Words: technetium-99m-DMSA; thallium-201-chloride; histologic malignancy; brain tumor; retention index; SPECT

J Nucl Med 1997; 38:1741–1749

CT and MRI can demonstrate smaller lesions due to their fine spatial resolution. Furthermore, their contrast enhancement, mainly dependent upon disrupted blood brain barrier (BBB), has been used to localize the tumors, but prediction of histopathological diagnosis was very difficult. Thallium-201-chloride, one of the most widely used radiopharmaceuticals, has been reported to differentiate, to some extent, benign lesions from malignant lesions of the lung (*1*), thyroid gland (*2*) and brain tumors (*3–7*), depending upon the uptake ratio and prolonged washout phase of radiotracer from the tumor tissue (*5–7*).

Pentavalent ^{99m}Tc(V)-DMSA was developed for a tumor imaging agent (*8,9*) and its accumulation has been reported in

Received Sep. 10, 1996; revision accepted Feb. 28, 1997.
For correspondence or reprints contact: Tsuneo Hirano, MD, 3-13-5 Showa-machi, Maebashi, Gunma 00371, Japan.

the medullary carcinoma of the thyroid (*10*), soft tissue tumors (*11,12*), lung cancers (*13*), osseous metastatic tumors (*13,14*) and primary brain tumors (*15*). We have established a simple and easy method to prepare ^{99m}Tc(V)-DMSA from a commercially available DMSA kit (*16*) and have imaged brain tumors to assess clinical usefulness in comparison to ^{201}TlCl.

We thought that there were several factors affecting tumor uptake, but only the prolonged washout phase might be specific to tumor histology and malignancy grade. Uptake ratios (early and delayed), retention ratio and retention index were calculated to evaluate and differentiate tumor specific components from nontumor specific ones. These numerical values of both radiopharmaceuticals were compared statistically with tumor histology and histologic grade of the brain tumors.

MATERIALS AND METHODS

Patients

Patients with a brain tumor on CT and/or MRI were selected for this study. Technetium-99m(V)-DMSA and ^{201}TlCl SPECT studies were performed prior to the surgical resection or stereotactic biopsy. Tumor size was measured by surgical specimen, contrast enhanced CT and gadolinium-DTPA enhanced MR images. Tumor vascularity was also evaluated by dynamic SPECT images (^{123}I-IMP, ^{99m}Tc-HMPAO or ^{99m}Tc-ECD), contrast enhanced CT and gadolinium-DTPA enhanced MR images, and classified into three groups: hypervascular, normovascular and hypovascular tumors.

Final diagnosis was made by histopathology of the specimens obtained by surgical procedure or stereotactic biopsy according to the WHO histological classification: glioblastoma, anaplastic astrocytoma (astrocytoma grade III), astrocytoma (astrocytoma grade II), pilocytic astrocytoma (astrocytoma grade I), meningioma and schwannoma.

Imaging

Technetium-99m(V)-DMSA was prepared using a commercially available dimercaptosuccinic acid (DMSA) kit. In brief, the Techne® DMSA kit contains 1.4 mg dimercaptosuccinic acid and 0.5 mg $SnCl_2 \cdot 2H_2O$. A DMSA kit, added with 200 μl of 7% of sodium bicarbonate solution ($NaHCO_3$), was reconstituted with 2 ml of ^{99m}Tc pertechnetate solution (approximately 740 MBq) (*16*).

Dynamic, early and delayed static SPECT images of the brain were obtained immediately, 30 min and 3 hr after intravenous administration of radiopharmaceuticals, using a ring-type SPECT scanner dedicated for brain study. Approximately 555 MBq ^{99m}Tc(V)-DMSA and 111 MBq ^{201}TlCl were administered intravenously, and these studies were performed on separate days within a week. Image acquisition was performed using 64 × 64 matrix with a 20% symmetric window at 140 KeV for ^{99m}Tc(V)-DMSA and 74 KeV for ^{201}TlCl. Acquisition time was 7.5 and 9 min per slice on early and delayed static images of ^{99m}Tc(V)-DMSA and 18 and 24 min on early and delayed static images of ^{201}TlCl, respectively. Butterworth and Ramachandran filters were used to reconstruct images in the transverse plane. Each image was corrected for tissue attenuation with the standard method (Sorenson method) using ^{99m}Tc pertechnetate or ^{201}TlCl in a phantom. In-plane spatial resolution was 9.6 mm (FWHM).

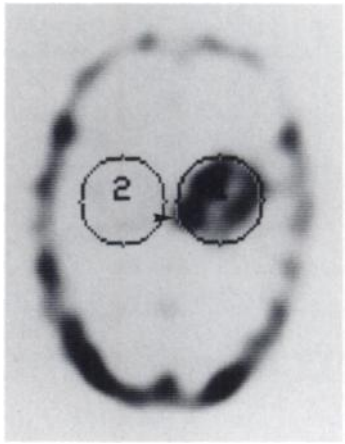

FIGURE 1. A circular region of interest (ROI) is drawn over the lesion of the greatest activity (arrowhead) and contralateral normal brain tissue.

Image Analysis

Both ^{99m}Tc(V)-DMSA and ^{201}TlCl SPECT images were compared with CT, MR images and tumor histology. Accumulation in the brain tumors was evaluated on SPECT images visually and a circular region of interest (ROI) was drawn over the site of the greatest activity in the lesion (L) (Fig. 1). A homologous ROI was drawn over the contralateral normal brain tissue (N) of the similar location. Maximum and average counts were obtained and uptake ratios (early and delayed), retention ratio and retention index were calculated on both early and delayed SPECT images (*1*).

Maximum counts were average of higher counts of adjacent 10 pixels in the ROI over the lesion (L) and contralateral normal region (N). Mean counts were the average of the total counts of the whole ROI over the lesion (L) and the contralateral normal tissue (N). The retention indices were calculated and evaluated in four combinations of maximum and mean counts; maximum counts of the lesion/maximum counts of the normal tissue (Max/Max), maximum counts of the lesion/mean counts of the normal tissue (Max/Mean), mean counts of the lesion/maximum counts of the normal tissue (Mean/Max), and mean counts of the lesion/mean counts of the normal tissue (Mean/Mean) in 20 lesions. There was some difference in the early and delayed uptake ratio depending on whether to choose maximum counts or mean counts of ROI (Table 1), however, there was no significant difference in the retention indices between maximum counts of the lesion/mean counts of the normal tissue and mean counts of the lesion/mean counts of the normal tissue, and between maximum counts of the lesion/maximum counts of the normal tissue and mean counts of the lesion/

TABLE 1
DMSA Uptake Ratios and Retention Index (Mean ± s.d.) of 20 Lesions

Method	Early uptake ratio Mean ± s.d.	Delayed uptake ratio Mean ± s.d.	Retention ratio Mean ± s.d.	Retention index Mean ± s.d.
Max/Max	2.90 ± 1.05	3.62 ± 0.98	0.72 ± 1.09	32.27 ± 39.32
Max/Mean	4.05 ± 2.04	6.00 ± 1.92	1.96 ± 1.51	61.40 ± 49.28
Mean/Max	2.24 ± 0.75	2.71 ± 0.73	0.47 ± 0.76	25.82 ± 33.02
Mean/Mean	3.12 ± 1.49	4.47 ± 1.35	1.42 ± 1.13	55.69 ± 49.17

Max/max = maximum counts of the lesion over maximum counts of the normal tissue.
Max/mean = maximum counts of the lesion over mean counts of the normal tissue.
Mean/max = mean counts of the lesion over maximum counts of the normal tissue.
Mean/mean = mean counts of the lesion over mean counts of the normal tissue.

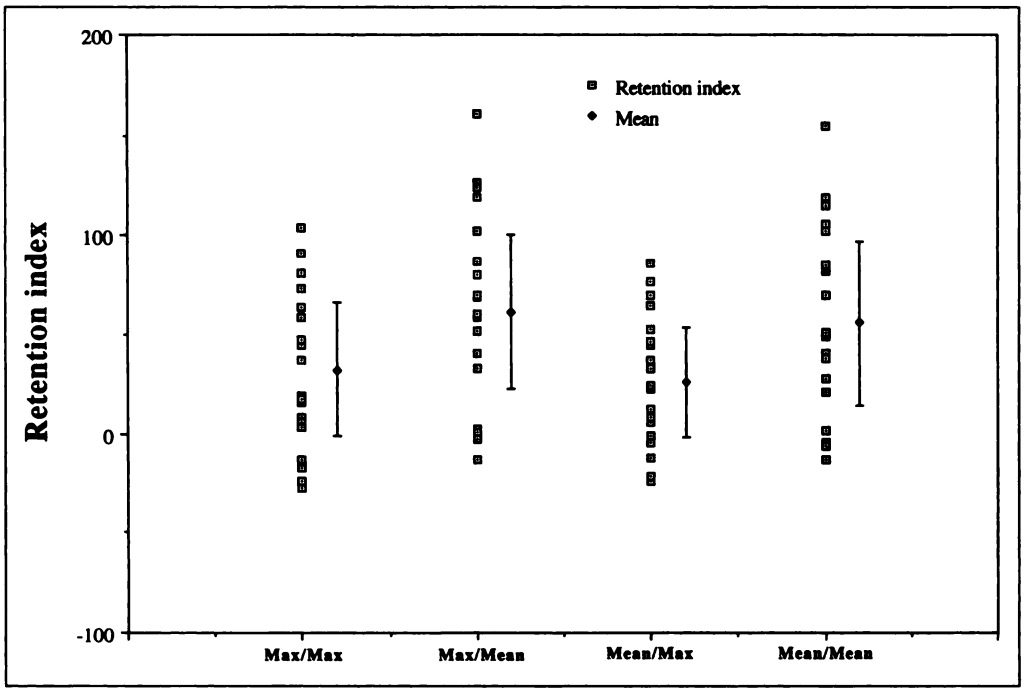

FIGURE 2. Retention index is calculated by 4 combinations of maximum and mean counts of ROI over the lesion and contralateral normal tissue in 20 cases. There is no significant difference between maximum counts of the lesion/mean counts of the normal tissue and mean counts of the lesion/mean counts of the normal tissue, and between maximum counts of the lesion/maximum counts of the normal tissue and mean counts of the lesion/maximum counts of the normal tissue because of making a ratio between early and delayed uptake.

maximum counts of the normal tissue (Fig. 2) because of making ratio between early and delayed uptake ratio.

Since a malignant tumor may often involve heterogeneous tissues, such as highly malignant tissue, normal residual tissue, necrotic tissue and so on, and the most aggressive part of the tumor might be represented by the area of maximum counts, we decided to normalize the maximum counts of the tumor to the average counts of the normal brain tissue. Maximum counts in the contralateral normal region may not reflect true homologous tissue, therefore, we calculated uptake ratio (L/N ratio) based on the maximum counts of the tumor normalized to the average counts of the homologous region (*7,13*) by their reproducibility.

Two uptake ratios (early and delayed) and retention ratio (delayed uptake ratio—early uptake ratio) were obtained for each brain tumor. Retention index was calculated as follows; [(delayed uptake ratio − early uptake ratio)/early uptake ratio)] × 100. Since we expected some difference in ^{99m}Tc(V)-DMSA and ^{201}TlCl uptake among the brain tumors, we compared uptake ratios, retention ratio and retention index with tumor histology and histologic malignancy grade using two-sided unpaired Student's t-test. Then ^{99m}Tc(V)-DMSA was evaluated in imaging quality, sensitivity and specificity compared to ^{201}TlCl.

RESULTS

One-hundred six studies were performed in 100 patients. One-hundred ten lesions of 118 (93.2%) and 104 lesions of 118 (88.1%) were positively demonstrated on ^{99m}Tc(V)-DMSA and ^{201}TlCl SPECT, respectively. There were 16 glioblastomas, 13 anaplastic astrocytomas (Grade III), 19 astrocytomas (Grade II), 29 meningiomas, 11 schwannomas, 14 metastases, 3 prolactinomas, 3 germinomas and 2 lymphomas. Of the primary and metastatic brain tumors, 93.2% were demonstrated on the ^{99m}Tc(V)-DMSA study. Seven astrocytomas (GII), (4 astrocytomas (GII), 1 fibrillary astrocytoma, 1 mixed oligoastrocytoma and 1 oligodendrogioma) and 1 epidermoid cyst were false negative. Of the brain tumors, 88.1% were positively demonstrated and false negative was seen in 1 astrocytoma (GIII), 9 astrocytomas (GII), 1 prolactinoma, 1 epidermoid cyst, 1 meningioma and 1 metastasis on ^{201}TlCl. Mixed gliomas (with no anaplasia) were provisionally classified into astrocytoma (GII) on this statistical analysis. Tables 2 and 3 present early and delayed uptake ratios, retention ratio and retention index of ^{99m}Tc(V)-DMSA and ^{201}TlCl, respectively.

There was no statistically significant difference between benign and malignant tumors on the early uptake ratio (mean ± s.d.) of ^{99m}Tc(V)-DMSA (Fig. 3). Only metastases (2.48 ± 1.00) were differentiated from meningiomas (3.43 ± 1.59) ($p < 0.05$) and schwannomas (3.34 ± 0.76) ($p < 0.03$). The early uptake ratio was very high in meningiomas (3.01 ± 1.71) and low in astrocytomas (GII) (1.61 ± 0.75) on ^{201}TlCl, and there was a statistically significant difference between meningiomas and glioblastomas (1.89 ± 0.46) ($p < 0.02$), meningiomas and astrocytomas (GII) ($p < 0.002$), and meningiomas and metastases (1.78 ± 0.35) ($p < 0.02$) (Fig. 3). There was no statistically significant difference between benign [astrocytomas (GII), meningiomas, schwannomas] and malignant glioblastomas, astrocytomas (GIII), metastases) tumors.

The delayed uptake ratio (Table 2) was high in glioblastomas (6.55 ± 2.60) and astrocytomas (GIII) (6.54 ± 3.63), and low in astrocytomas (GII) (3.14 ± 2.36) and meningiomas (3.85 ± 1.88) on ^{99m}Tc(V)-DMSA (Fig. 4), and specific to the histological malignancy with statistically significant difference ($p < 0.04$) between malignant tumors [glioblastomas (6.55 ± 2.60), astrocytomas (GIII) (6.54 ± 3.63), metastases (5.86 ± 2.60)] and benign tumors [astrocytomas (GII) (3.14 ± 2.36), meningiomas (3.85 ± 1.88), schwannomas (4.03 ± 1.11)]. On ^{201}TlCl (Table 3), the delayed uptake ratio (Fig. 4) was high in meningiomas (2.47 ± 0.88) and low in astrocytomas (GII) (1.54 ± 0.70), and there was statistically significant difference between glioblastomas (2.03 ± 0.39) and astrocytomas (GII) (1.54 ± 0.70) ($p < 0.02$), astrocytomas (GIII) (2.09 ± 0.76) and astrocytomas (GII) ($p < 0.05$), astrocytomas (GII) and meningiomas ($p < 0.0003$), astrocytomas (GII) and schwannomas (2.16 ± 0.68) ($p < 0.03$) and meningiomas and metastases (1.86 ± 0.44) ($p < 0.02$). It was difficult to differentiate malignant tumors from benign ones.

The retention ratio (Table 2) of ^{99m}Tc(V)-DMSA was high in malignant tumors [glioblastomas (3.34 ± 1.54), astrocytomas (GIII) (3.26 ± 2.19), metastases (3.37 ± 1.75)] and low in benign tumors [astrocytomas (GII) (0.67 ± 0.75), meningiomas (0.39 ± 0.51) and schwannomas (0.69 ± 0.90)] with a

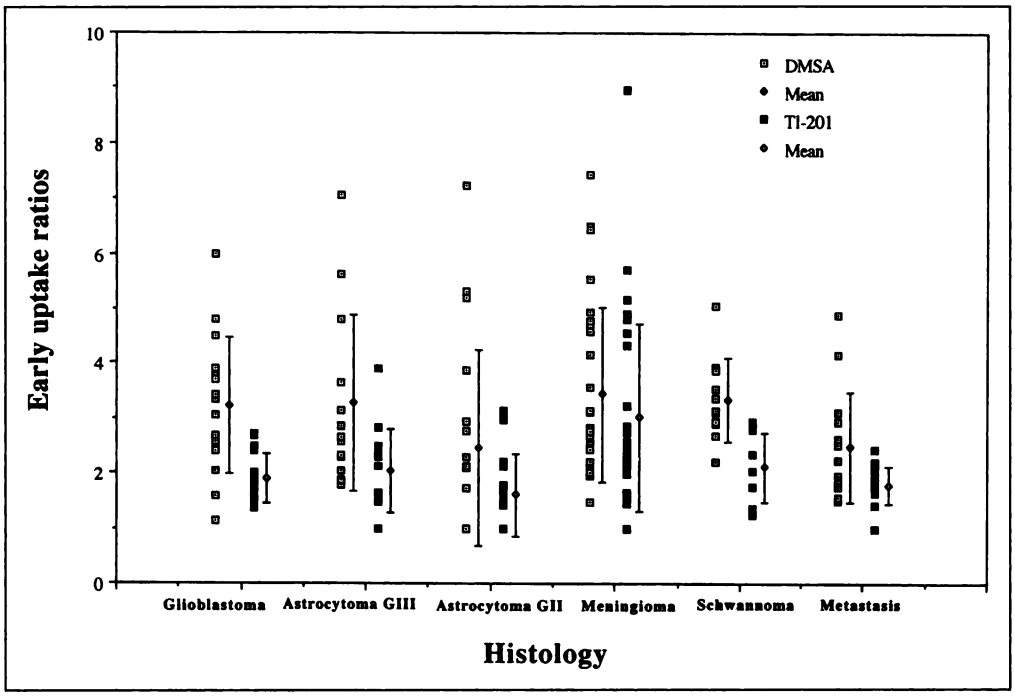

FIGURE 3. Early uptake ratio of ^{99m}Tc(V)-DMSA and ^{201}TlCl: There is no statistically significant difference between benign and malignant tumors on either ^{99m}Tc(V)-DMSA or ^{201}TlCl.

statistically significant difference ($p < 0.002$) (Fig. 5). On ^{201}TlCl (Table 3), the retention ratio was high in glioblastomas (0.14 ± 0.20) and low in meningiomas (-0.51 ± 0.99). Meningiomas were differentiated from glioblastomas ($p < 0.02$), astrocytomas (GIII) (0.06 ± 0.24) ($p < 0.05$) and metastases (0.08 ± 0.29) ($p < 0.04$). Astrocytomas (GII) (-0.07 ± 0.25) were differentiated from glioblastomas ($p < 0.02$) (Fig. 5). There was no statistically significant difference between benign and malginant tumors.

The retention index (Table 2) of ^{99m}Tc(V)-DMSA was very high in glioblastomas (103.4 ± 35.47), astrocytomas (GIII) (96.35 ± 37.49) and metastases (137.55 ± 49.78), but low in astrocytomas (GII) (22.66 ± 24.91), meningiomas (10.88 ± 13.02) and schwannomas (22.18 ± 29.32) (Fig. 6). There was a statistically significant difference between malignant tumors [glioblastomas, astrocytomas (GIII), and metastases] and benign tumors [astrocytomas (GII), meningiomas and schwannomas] ($p < 0.0001$), glioblastomas and metastases ($p < 0.04$), astrocytomas (GII) and metastases ($p < 0.03$), and astrocytomas (GII) and meningiomas ($p < 0.04$), but there was no significant difference between glioblastomas and astrocytomas (GIII), astrocytomas (GII) and schwannomas, or meningiomas and schwannomas. On ^{201}TlCl (Table 3), the retention index was high in glioblastomas (9.08 ± 11.04) and very low in meningiomas (-11.01 ± 20.19). Meningiomas were differentiated from glioblastomas (9.08 ± 11.04) ($p < 0.007$), astrocytomas (GIII) (3.02 ± 9.68) ($p < 0.03$), schwannomas (3.61 ± 8.44) ($p < 0.03$), and metastases (4.26 ± 14.00) ($p < 0.02$). Astrocytomas (GII) (-2.77 ± 9.85) were differentiated from glioblastomas ($p < 0.002$) (Fig. 6). There was no statistically significant difference between benign and malignant tumors.

Tumor vascularity was evaluated by contrast enhanced CT, gadolinium-DTPA enhanced MR images and dynamic SPECT images. High-grade astrocytomas, meningiomas and schwannomas tended to be hypervascular, but low-grade astrocytomas and metastatic carcinomas tended to be less vascular. Hypervascular tumors were clearly demonstrated on both early and delayed images of ^{99m}Tc(V)-DMSA and ^{201}TlCl (Fig. 7). On the delayed images, glioblastomas and most of the astrocytomas (GIII) (Fig. 8) were more distinctly visible and showed significantly higher uptake than on the early ones, but meningiomas (Fig. 7) and schwannomas showed similar or slightly higher uptake ratios than on the early ones. Therefore, calculated retention ratio and retention index were high in glioblastomas and astrocytomas (GIII), but low in meningiomas and schwannomas on ^{99m}Tc(V)-DMSA. Normo- or hypo-vascular tumors tended to show mildly or slightly increased uptake on the early images. Metastases (Fig. 9) and most of the astrocytomas (GIII)

TABLE 2
DMSA Uptake Ratios and Retention Index (Mean ± s.d.) of 110 Lesions

Histology	Number of lesions demonstrated	Early uptake ratio (Mean ± s.d.)	Delayed uptake ratio (Mean ± s.d.)	Retention ratio (Mean ± s.d.)	Retention index (Mean ± s.d.)
Glioblastoma	16	3.21 ± 1.25	6.55 ± 2.60	3.34 ± 1.54	103.40 ± 35.47
Astrocytoma (G III)	13	3.28 ± 1.61	6.54 ± 3.63	3.26 ± 2.19	96.35 ± 37.49
Astrocytoma (G II)*	19	2.46 ± 1.78	3.14 ± 2.36	0.67 ± 0.75	22.66 ± 24.91
Meningioma	29	3.43 ± 1.59	3.85 ± 1.88	0.39 ± 0.51	10.88 ± 13.02
Schwannoma	11	3.34 ± 0.76	4.03 ± 1.11	0.69 ± 0.90	22.18 ± 29.32
Metastasis	14	2.48 ± 1.00	5.86 ± 2.60	3.37 ± 1.75	137.55 ± 49.78
Prolactinoma	3	6.09 ± 5.72	8.74 ± 8.37	2.64 ± 2.65	41.60 ± 3.05
Germinoma	3	2.79 ± 1.31	4.14 ± 1.51	1.36 ± 0.26	54.63 ± 22.81
Lymphoma	2	2.04 ± 0.61	3.65 ± 0.76	1.61 ± 0.16	81.4 ± 16.7

*Mixed gliomas were classified into astrocytoma (G II) for statistical analysis.

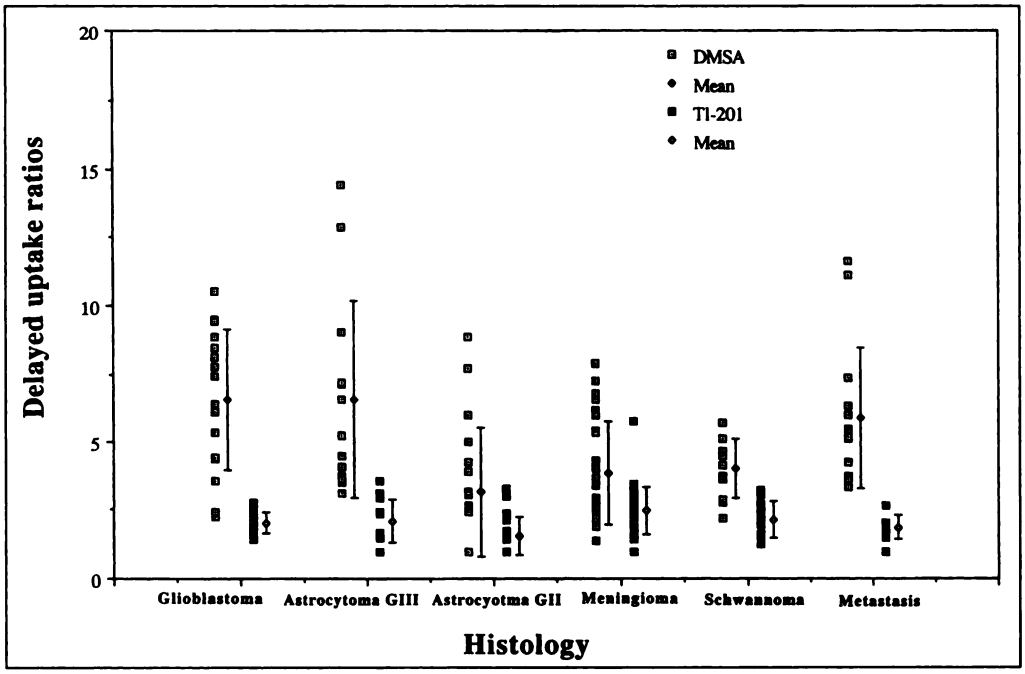

FIGURE 4. Delayed uptake ratio of ^{99m}Tc(V)-DMSA and ^{201}TlCl: There is a statistically significant difference ($p < 0.04$) between benign [astrocytomas (GII), meningiomas and schwannomas] and malignant [glioblastomas, astrocytomas (GIII) and metastases] tumors on ^{99m}Tc(V)-DMSA, but there is no statistically significant difference between benign and malignant tumors on ^{201}TlCl.

(Fig. 8) showed markedly increased uptake in comparison to the surrounding normal tissue on the delayed images, but astrocytomas (GII) showed mildly increased or less uptake on the delayed images (Fig. 10). Therefore, calculated retention ratio and index were high in astrocytomas (GIII) and metastases, but low in astrocytomas (GII). On ^{201}TlCl, the retention ratio and index were very similar to the pattern of the early and delayed uptake ratios, except for higher in glioblastomas and lower in meningiomas.

DISCUSSION

The early uptake ratio could be modified by the various factors not specific to the tumor histology or histologic malignancy grade, and reflect mainly blood perfusion. The early uptake ratio was slightly low in astrocytomas (GII) (2.46 ± 1.75) and metastases (2.48 ± 1.00) on ^{99m}Tc(V)-DMSA, and high in meningiomas (3.01 ± 1.71), but low in astrocytomas (GII) (1.61 ± 0.75) and metastases (1.78 ± 0.35) on ^{201}TlCl. These findings were roughly consistent with the degree of enhancement on both the MRI and CT and with the perfusion on the dynamic SPECT images. There was no statistically significant difference between benign and malignant tumors on either ^{99m}Tc(V)-DMSA or ^{201}TlCl. The early uptake ratio of ^{99m}Tc(V)-DMSA did not show any significant difference among the tumors. Only meningiomas could be differentiated from glioblastomas, astrocytomas (GII) and metastases by their high early uptake ratio of ^{201}TlCl. These differences may suggest that there are different mechanism of tumor uptake between ^{99m}Tc(V)-DMSA and ^{201}TlCl. Although several papers have reported that gliomas could be differentiated by the early uptake ratio of ^{201}TlCl (*3–6*), there was no statistically significant difference among the gliomas and their histological malignancy grade could not be differentiated on our analysis.

The change of the delayed uptake ratio was dependent upon the washout from the early uptake, therefore, it became more specific to the tumor histology than the early uptake ratio, but still less specific than the retention index because of some modification by the various factors comprising the early uptake ratio. For example, a hypervascular lesion showed a higher delayed uptake ratio than a less vascular lesion with same washout rate. The delayed uptake ratio was low in the benign tumors [astrocytomas (GII) (3.14 ± 2.36), meningiomas (3.85 ± 1.88) and schwannomas (4.03 ± 1.11)] and high in the malignant tumors [glioblastomas (6.55 ± 2.60), astrocytomas (GIII) (6.54 ± 3.63) and metastases (5.86 ± 2.60)]. Benign and malignant tumors could be differentiated with a statistically significant difference ($p < 0.04$) on ^{99m}Tc(V)-DMSA. The delayed uptake ratio tended to be high in the malignant tumors, especially in the metastases, which was low in the early uptake

TABLE 3
Thallium-201-Chloride Uptake Ratios and Retention Index (Mean ± s.d.) of 110 Lesions

Histology	Number of lesions demonstrated	Early uptake ratio (Mean ± s.d.)	Delayed uptake ratio (Mean ± s.d.)	Retention ratio (Mean ± s.d.)	Retention index (Mean ± s.d.)
Glioblastoma	16	1.89 ± 0.46	2.03 ± 0.39	0.14 ± 0.20	9.08 ± 11.04
Astrocytoma (GIII)	13	2.03 ± 0.76	2.09 ± 0.76	0.06 ± 0.24	3.02 ± 9.68
Astrocytoma (GII)*	19	1.61 ± 0.75	1.54 ± 0.70	−0.07 ± 0.25	−2.77 ± 9.85
Meningioma	29	3.01 ± 1.71	2.47 ± 0.88	−0.51 ± 0.99	−11.01 ± 20.19
Schwannoma	11	2.12 ± 0.63	2.16 ± 0.68	0.04 ± 0.17	3.61 ± 8.44
Metastasis	14	1.78 ± 0.35	1.86 ± 0.44	0.08 ± 0.29	4.26 ± 14.00
Prolactinoma	3	3.13 ± 1.91	3.54 ± 2.26	0.42 ± 0.36	10.13 ± 9.00
Germinoma	3	1.64 ± 0.38	1.80 ± 0.09	0.17 ± 0.47	14.50 ± 28.12
Lymphoma	2	2.93 ± 0.40	3.16 ± 0.42	0.23 ± 0.02	7.70 ± 0.31

*Mixed gliomas were classified into astrocytoma (GII) for statistical analysis.

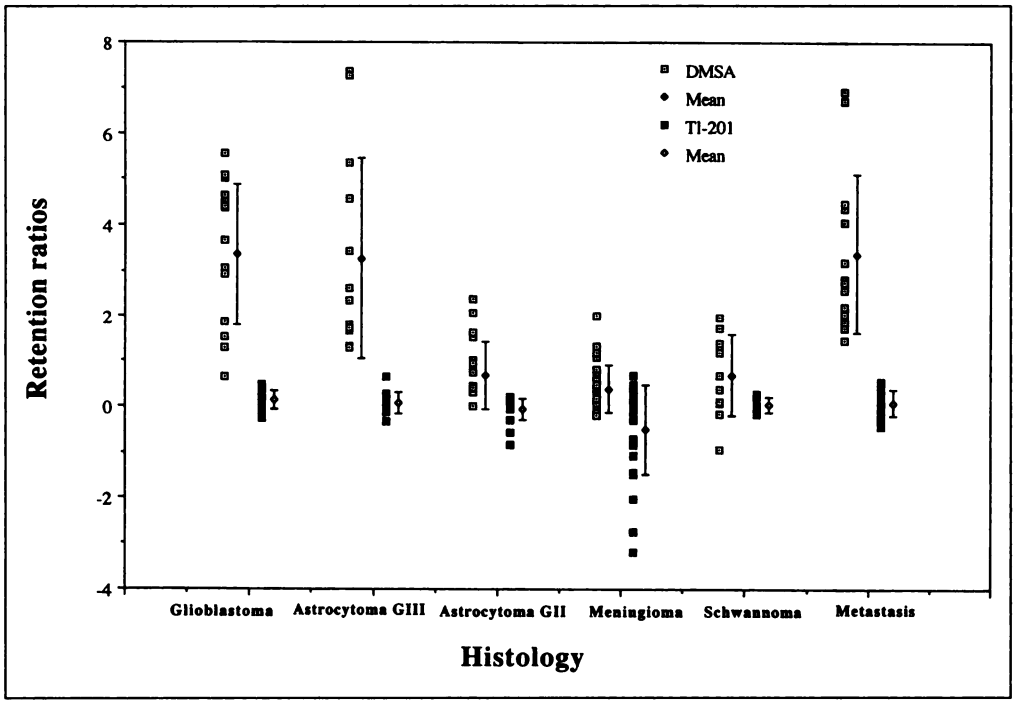

FIGURE 5. Retention ratio of ^{99m}Tc(V)-DMSA and ^{201}TlCl: There is a statistically significant difference ($p < 0.002$) between benign [astrocytomas (GII), meningiomas and schwannomas] and malignant [glioblastomas, astrocytomas (GIII) and metastases] tumors on ^{99m}Tc(V)-DMSA, but there is no statistically significant difference between benign and malignant tumors on ^{201}TlCl.

ratio (2.48 ± 1.00) and high in the delayed uptake ratio (5.86 ± 2.60). Such a significant change from the early uptake ratio could differentiate between benign and malignant tumors. On ^{201}TlCl, the delayed uptake ratio was low in astrocytomas (GII) (1.54 ± 0.70) and metastases (1.86 ± 0.44), and high in glioblastomas (2.03 ± 0.39), astrocytomas (GIII) (2.09 ± 0.76), meningiomas (2.47 ± 0.88) and schwannomas (2.16 ± 0.68). The delayed uptake ratio (Fig. 4) was very similar to the early uptake ratio (Fig. 3) in both benign and malignant tumors, except for that of meningiomas because of their fast washout, and the delayed uptake ratio could not differentiate between benign and malignant tumors.

The retention ratio was calculated by subtracting the early uptake ratio from the delayed uptake ratio, and then the factors affecting the early uptake ratio would decrease in the retention ratio. The retention ratio was very high in malignant tumors [glioblastomas (3.34 ± 1.54), astrocytomas (GIII) (3.26 ± 2.19) and metastases (3.37 ± 1.75)], and very low in benign tumors [astrocytomas (GII) (0.67 ± 0.75), meningiomas (0.39 ± 0.51) and schwannomas (0.69 ± 0.90)] on ^{99m}Tc(V)-DMSA. Malignant tumors could be differentiated from benign tumors with a statistically significant difference ($p < 0.002$). On ^{201}TlCl, the retention ratio was very low, especially in the astrocytomas (GII) (−0.07 ± 0.25) and meningiomas (−0.51 ± 0.99). Astrocytomas (GII) were differentiated from glioblastomas (0.14 ± 0.20) ($p < 0.02$), and meningiomas (−0.51 ± 0.99) ($p < 0.03$) were differentiated from glioblastomas ($p < 0.02$), astrocytomas (GIII) (0.06 ± 0.24) ($p < 0.05$) and metastases (0.08 ± 0.29) ($p < 0.04$). The delayed uptake ratio could not differentiate between benign and malignant tumors.

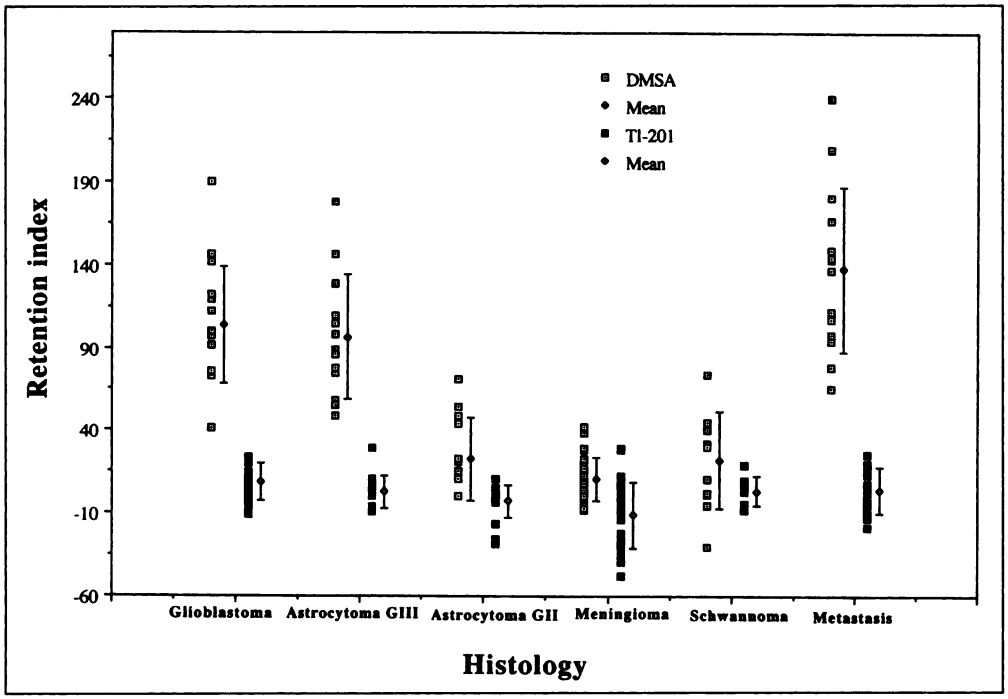

FIGURE 6. Retention index of ^{99m}Tc(V)-DMSA and ^{201}TlCl: There is a statistically significant difference ($p < 0.0001$) between benign [astrocytomas (GII), meningiomas and schwannomas] and malignant [glioblastomas, astrocytomas (GIII) and metastases] tumors on ^{99m}Tc(V)-DMSA, but there is no statistically significant difference between benign and malignant tumors on ^{201}TlCl.

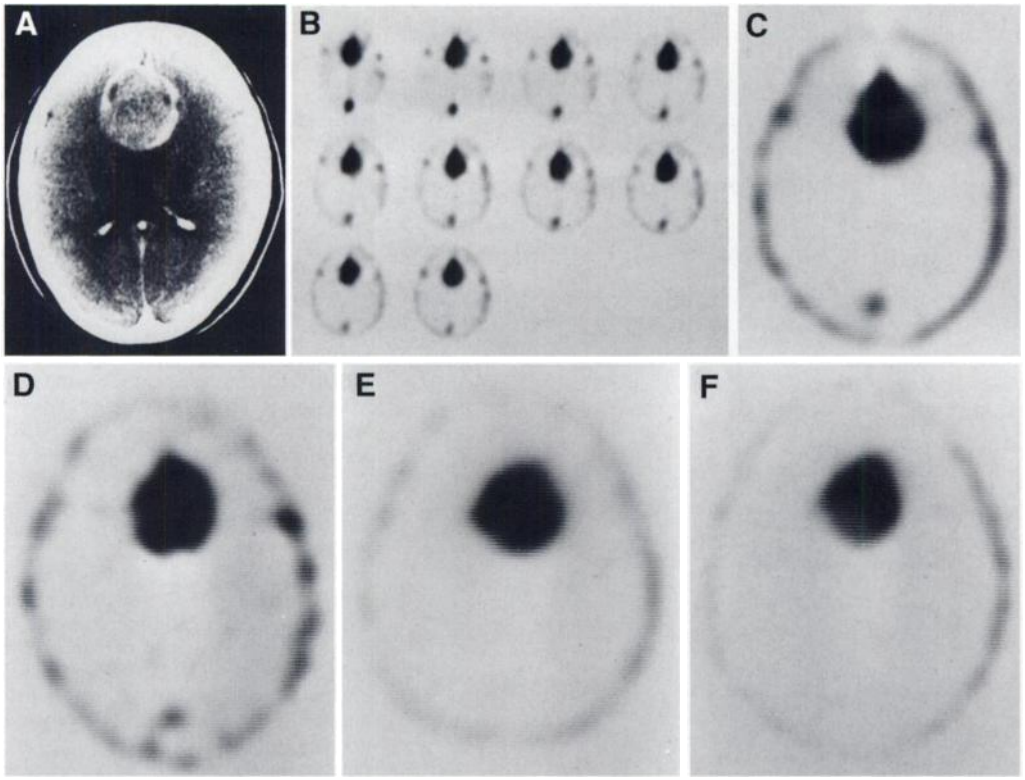

FIGURE 7. Meningioma: Contrast enhanced CT (A), ^{99m}Tc(V)-DMSA dynamic (B), early (C) and delayed (D) static images and ^{201}TlCl early (E) and delayed (F) static images: There is a large round contrast-enhanced lesion in the frontal lobe on contrast enhanced CT image (A). Technetium-99m(V)-DMSA dynamic images (B) show a large area of intense uptake in the frontal lobe. There is a large area of increased uptake on both early (C) and delayed (D) static image with a calculated retention index of 0.77. There is a large area of increased uptake on both early (E) and delayed (F) static image with a calculated retention index of −35.6.

The retention index was calculated by dividing the retention ratio by the early uptake ratio, therefore, the retention index reflected the washout phase and could clearly differentiate between benign and malignant brain tumors. These differentiations would depend solely on the prolonged washout phase, which was very specific to the tumor malignancy and histologic grade. The retention index was very high in the malignant tumors [glioblastomas (103.40 ± 35.47), astrocytomas (GIII) (96.35 ± 37.49) and metastases (137.55 ± 49.78)], and low in the benign tumors [astrocytomas (GII) (22.66 ± 24.91), meningiomas (10.88 ± 13.02) and schwannomas (22.18 ± 29.32)] on ^{99m}Tc(V)-DMSA. The benign tumors were easily differentiated from the malignant tumors with a statistically significant difference ($p < 0.0001$). There was no significant difference between glioblastomas and astrocytomas (GIII), astrocytomas (GII) and schwannomas, or meningiomas and schwannomas ($p > 0.05$).

In the metastases, the early uptake ratio was low, but the retention index was the highest in the tumors. On ^{201}TlCl, the retention index was high in the glioblastomas (9.08 ± 11.04)

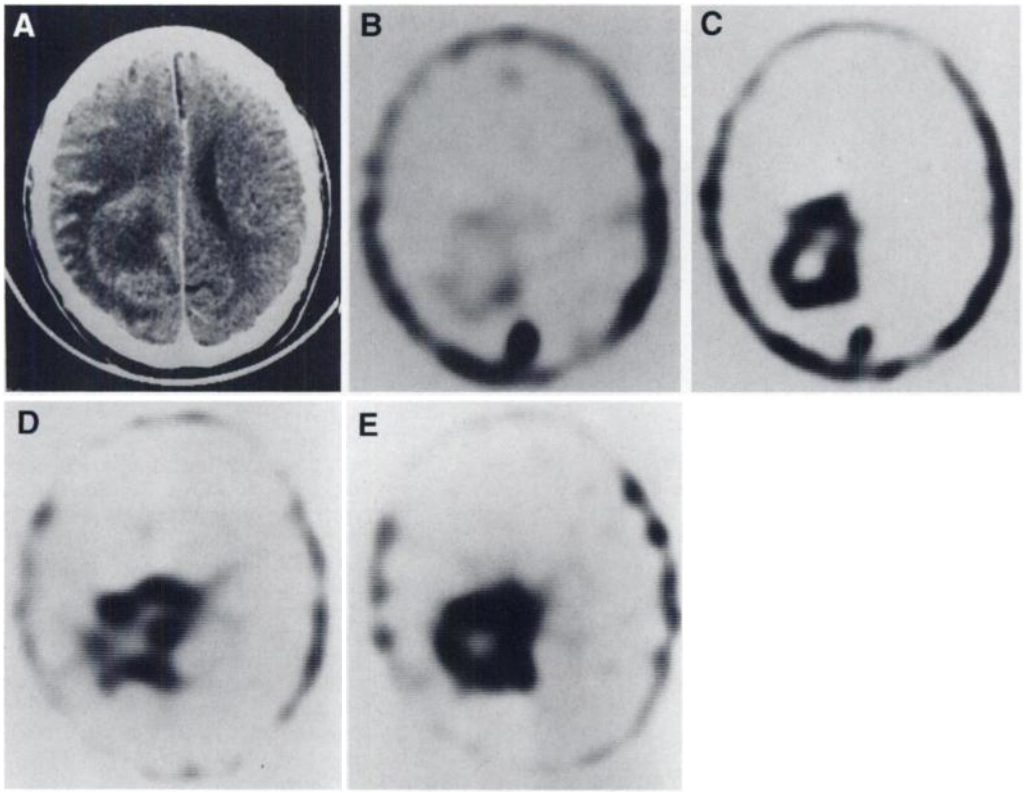

FIGURE 8. Astrocytoma (GIII); Contrast enhanced X-CT (A), ^{99m}Tc(V)-DMSA early (B) and delayed (C) static images, and ^{201}TlCl early (D) and delayed (E) static images: There is a large irregular ring-like enhancement noted in the right fronto-parietal lobe on contrast CT image. Technetium-99m(V)-DMSA SPECT shows a ring-like area of slightly increased uptake in the right fronto-parietal lobe on the early static image (B). There is a ring-like area of moderately increased uptake on the delayed static image (C) with high calculated retention index of 109. Thallium-201-chloride SPECT shows a ring-like area of mildly increased uptake on the early static image (D) and moderately increased uptake on the delayed static image (E) with calculated retention index of 9.19.

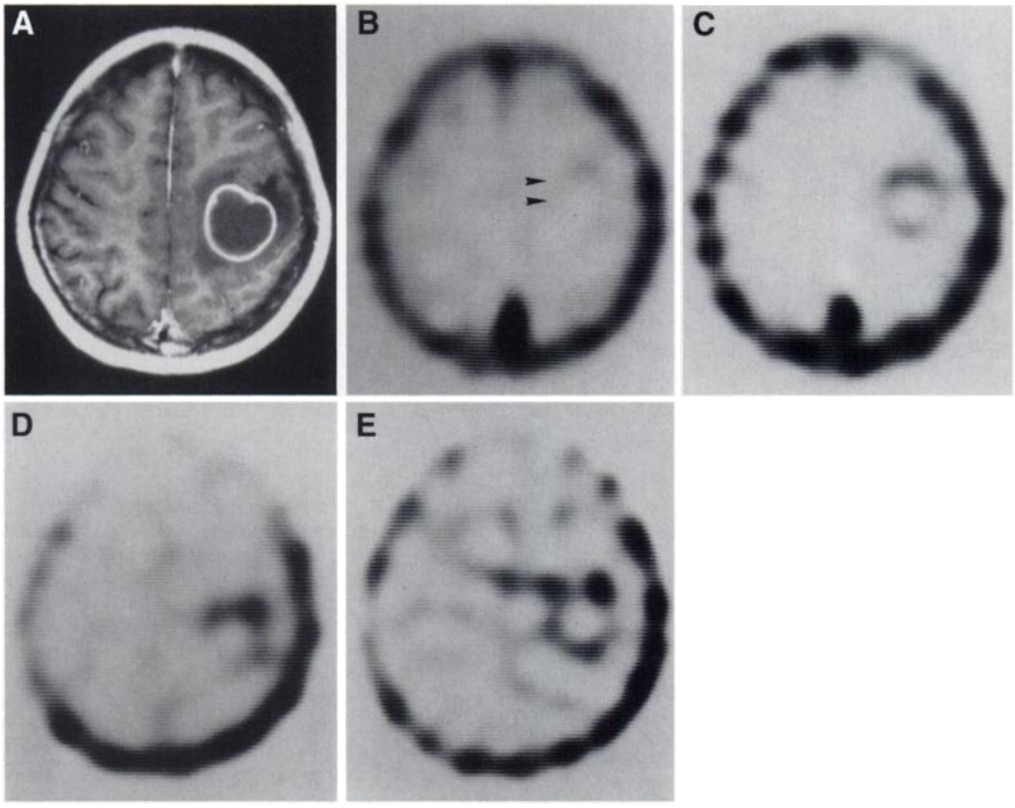

FIGURE 9. Metastasis: Gd-enhanced MRI (A), ^{99m}Tc(V)-DMSA early (B) and delayed (C) static images, and ^{201}TlCl early (D) and delayed (E) static images: There is a ring-like Gd-enhancemelit in the left fronto-parietal region on MR (TR: 440 ms, TE: 15 ms) image (A). Technetium-99m(V)-DMSA SPECT shows a ring-like area of faintly increased uptake in the left fronto-parietal region (arrow) on the early static image (B) and a ring-like area of mildly increased uptake on the delayed static image (C) with calculated retention index of 144. Thallium-201-chloride SPECT shows a mildly increased ring-like uptake on both early (D) and delayed (E) static images with calculated retention index of −4.27.

and low in the meningiomas (−11.01 ± 20.19). Glioblastomas were differentiated from astrocytomas (GII) (−2.77 ± 9.85) ($p < 0.002$), and meningiomas were differentiated from glioblastomas ($p < 0.0007$), astrocytomas (GIII) (3.02 ± 9.68) ($p < 0.03$), schwannomas (3.61 ± 8.44) ($p < 0.03$) and metastases (4.26 ± 14.00) ($p < 0.02$). The retention index had a large standard deviation and could not differentiate between benign and malignant tumors.

On ^{99m}Tc(V)-DMSA, the early uptake ratio was slightly low in astrocytomas (GII) and metastases, but there was no statistically significant difference between benign and malignant tumors. The delayed uptake ratio became high in malignant tumors and low in benign tumors, and the retention ratio became higher in malignant tumors and lower in benign tumors. The retention index clearly differentiated benign tumors from malignant tumors with a statistically significant difference ($p < 0.0001$). On ^{201}TlCl, the early uptake ratio was middle, and the delayed uptake ratio, retention ratio and retention index were high in glioblastomas. The early uptake ratio, delayed uptake ratio, retention ratio and retention index were all low in

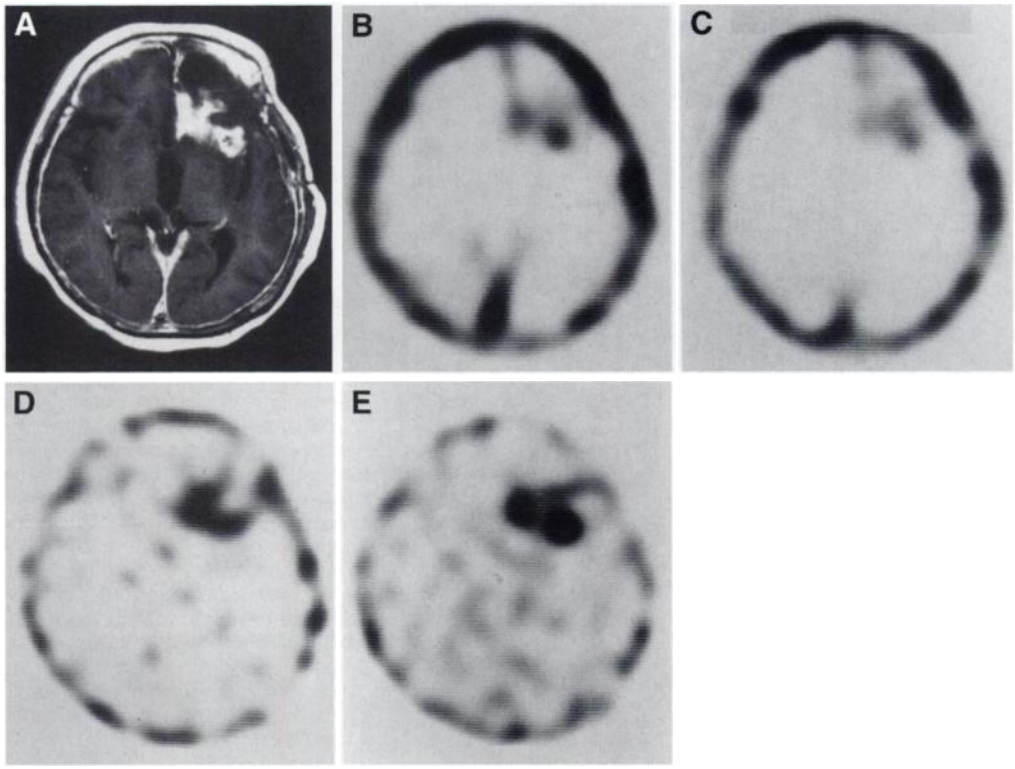

FIGURE 10. Astrocytoma (GII); Gd-enhanced MRI (A), ^{99m}Tc(V)-DMSA early (B) and delayed (C) static images, and ^{201}TlCl early (D) and delayed (E) static images: MR (TR:440 ms, TE: 15 ms) image shows irregular enhancement with cystic components in the left frontal lobe. Technetium-99m(V)-DMSA SPECT shows an area of mildly increased uptake in the left frontal lobe on the early static image (B) and slightly increased uptake on the delayed static image (C) with calculated retention index of 14.5. Thallium-201-chloride SPECT shows mildly increased uptake on both early (D) and delayed (E) images with calculated retention index of −25.6.

astrocytomas (GII). The early uptake ratio and delayed uptake ratio were high, but retention ratio and retention index were lowest in meningiomas. The early uptake ratio and delayed uptake ratio were low, but the retention ratio and retention index were middle in metastases. Meningiomas were differentiated from other benign and malignant tumors by their high early and delayed uptake ratios, and low retention ratio and index. Astrocytomas (GII) were differentiated from glioblastomas by the delayed uptake ratio, retention ratio and retention index, and from astrocytomas (GIII) by the delayed uptake ratio. However, it was difficult for ^{201}TlCl to differentiate benign tumors from malignant ones and to evaluate histological malignancy grade, and also to differentiate malignancy grade even among the gliomas.

False negative cases were seen mostly in astrocytomas (GII) on both ^{99m}Tc(V)-DMSA and ^{201}TlCl, most likely due to their hypovascularity. But, ^{201}TlCl showed false negative in several other tumors.

CONCLUSION

Technetium-99m(V)-DMSA uptake was mainly dependent upon the tumor vascularity with no significant difference among the primary and metastatic brain tumors. Washout from the lesions was different from tumor to tumor and independent of tumor vascularity, but was closely related to tumor histology and histological malignancy. Thallium-201-chlorine uptake was also dependent on tumor vascularity, but showed no significant relationship between washout and tumor histology or histological malignancy. Therefore, differentiation between benign and malignant tumors was difficult by the uptake and retention of ^{201}TlCl. This may suggest that there should be different uptake and washout mechanisms between ^{201}TlCl and ^{99m}Tc(V)-DMSA. Technetium-99m(V)-DMSA could clearly demonstrate primary and metastatic brain tumors with a sensitivity of 93.2%, which is slightly higher than the 88.1% of ^{201}TlCl. False negative was very limited in astrocytomas (GII). Tumor histology and histological malignancy grade could also be predicted noninvasively by numerical scores, which would be very useful to determine the therapeutic methods. Technetium-99m(V)-DMSA was superior to ^{201}TlCl in imaging quality, sensitivity and specificity to tumor histology and histological malignancy of the primary and metastatic brain tumors.

REFERENCES

1. Tonami N, Shuke N, Yokoyama K, Seki H, et al. Thallium-201 single photon emission computed tomography in the evaluation of suspected lung cancer. *J Nucl Med* 1989;30:997–1004.
2. Tonami N, Hisada K. Clinical experience of tumor imaging with ^{201}Tl-chloride. *Clin Nucl Med* 1977;2:75–81.
3. Kaplan WD, Takvorian T, Morris JH, Rumbaugh CL, Connoly BT, Atkins HL. Thallium-201 brain tumor imaging: a comparative study with pathologic correlation. *J Nucl Med* 1987;28:47–52.
4. Ancri D, Bassett JY, Lonchampt MF, et al. Diagnosis of cerebral lesions by thallium-201. *Radiology* 1978;128:417–422.
5. Black KL, Hawkins RA, Kim KT, Becker DP, Lerner C, Marciano. Use of thallium-201 SPECT to quantitate malignancy grade of gliomas. *J Neurosurg* 1989; 71:342–346.
6. Mountz JM, Stafford-Schuck K, McKeever PE, Taren J, Beierwaltes WH. Thallium-201 tumor/cardiac ratio estimation of residual astrocytoma. *J Neurosurg* 1988;68:705–709.
7. Kim KT, Black KL, Marciano D, Mazziotta JC, Guze BH, Grafton S, Hawkins RA, Becker DP. Thallium-201 SPECT images of brain tumors: methods and results. *J Nucl Med* 1990;31:965–969.
8. Westera G, Gadze A, Horst W. A convenient method for the preparation of ^{99m}Tc(V) dimercaptosuccinic acid (^{99m}Tc(V)-DMSA). *Int J Appl Radiat Isot* 1985;36:311–312.
9. Blower PJ, Singh J, Clarke SEM. The chemical identity of pentavalent technetium-99m-dimercaptosuccinic acid. *J Nucl Med* 1991;32:845–849.
10. Ohta H, Yamamoto K, Endo K, et al. A new imaging agent for medullary carcinoma of the thyroid. *J Nucl Med* 1984;25:323–325.
11. Ohta H, Endo K, Fujita T, et al. Imaging of soft tissue tumors with Tc(V)-99m dimercaptosuccinic acid, A new tumor seeking agent. *Clin Nucl Med* 1984;9:568–573.
12. Ohta H, Endo K, Fujita T, Konishi J, Torizuka K, Horiuchi K, Yokoyama A. Clinical evaluation of tumor imaging using ^{99m}Tc(V) dimercaptosuccinic acid, a new tumor seeking agent. *Nucl Med Commun* 1988;9:105–116.
13. Hirano T, Otake H, Yoshida I, Endo K. Primary lung cancer SPECT imaging with pentavalent technetium-99m-DMSA. *J Nucl Med* 1995;36:202–207.
14. Lamki L, Shearer R. Tc-99m-DMSA uptake by metastatic carcinoma of the prostate. *J Nucl Med* 1985;25:733–734.
15. Hirano T, Otake H, Shibasaki T, Tamura M, Endo K. Differentiating histologic malignancy of primary brain tumors: pentavalent technetium-99m-DMSA. *J Nucl Med* 1997;38:20–26.
16. Hirano T, Tomiyoshi K, Ying Jian Zhang, Ishida T, Inoue T, Endo K. Preparation and clinical evaluation of ^{99m}Tc-DMSA for tumor scintigraphy. *Eur J Nucl Med* 1994;21:82–85.

Prediction of Myelotoxicity Using Semi-Quantitative Marrow Image Scores

S. Lim, G.L. DeNardo, D.A. DeNardo, R.T. O'Donnell, A. Yuan and S.J. DeNardo

University of California Davis Medical Center; and Veterans Administration Northern California Health Care System, Sacramento, California

Marrow radiation with resultant myelosuppression is usually dose-limiting in radioimmunotherapy (RIT). This study evaluated the relationship between a semiquantitative score of radiolabeled antibody marrow uptake obtained by imaging and subsequent decrease in peripheral blood cell counts in a patient population in whom marrow malignancy is common. **Methods:** Semiquantitative scores were assigned to lumbar marrow images of 18 patients acquired 0, 6, 24 and 48 hr after the first therapy dose of ^{131}I-Lym-1. Scores were adjusted for injected dose (GBq) and body surface area (m^2), and correlated with post-therapy blood counts. A well-defined scale, where 0 and 4 represented least to highest marrow uptake when compared to background, was used to assign marrow image scores. Injected doses of ^{131}I-Lym-1 ranged from 1.1–8.2 GBq (29–222 mCi). **Results:** Linear regression of summed marrow scores (0–24 hr after injection) versus decrease in cell counts produced correlation coefficients of 0.76, 0.44, 0.58 and 0.46 for platelets, granulocytes, white blood cells (WBC) and hematocrit, respectively. Scores for individual and other combinations of images obtained immediately up to 24 hr after injection were also predictive.

Key Words: myelotoxicity; marrow imaging; radioimmunotherapy; semiquantitative

J Nucl Med 1997; 38:1749–1753

Received Nov. 13, 1996; revision accepted Mar. 4, 1997.

For correspondence or reprints contact: G.L. DeNardo, MD, Molecular Cancer Institute, School of Medicine, University of California Davis Medical Center, 1508 Alhambra Blvd. #214, Sacramento, CA 95816.